N. Triantafyllidis
Mem. ASME

B. Maker

Aerospace Engineering Department,
The University of Michigan,
Ann Arbor, MI 48109

Shyam K. Samanta
Professor,
Dept. of Mechanical Engineering
and Applied Mechanics,
University of Michigan,
Ann Arbor, Mich. 48109-2125
Fellow ASME

An Analysis of Drawbeads in Sheet Metal Forming: Part I—Problem Formulation

The development of a one-dimensional finite strain elasto-plastic shell model appropriate for use in modelling straight drawbeads is outlined. Numerical results obtained using a finite element technique are shown for practical bead designs. The sheet deformation is divided into two phases: that when the binder locks the sheet metal to form the bead, and that when the punch advances to form the panel, pulling the sheet and (possibly) drawing material through the bead. The effects of friction coefficient, bead geometry, and material properties are investigated, resulting in strain distribution diagrams and force-displacement curves for several bead designs.

1 Introduction

A very critical element in the design of dies employed in sheet metal forming processes is the design of the drawbeads. During the forming operation these beads, which are situated in the blankholder/binder surface, provide the restraining force which controls the flow of metal into the die.

Previous studies in this area include the steady state experiments conducted by Nine [1], who used simplified bead geometry to investigate the various parameters affecting the restraining forces in the bead, and the modelling technique developed by Wang [2], which to date has been the only analytical investigation on the subject. In the latter work, however, the equilibrium equation in the direction normal to the sheet was ignored for analytical simplicity and only the steady state solution was investigated. In addition, a membrane approximation was employed for the calculation of the frictional forces, which is approximately valid only for the case of a circular bead.

It is the purpose of this work to investigate, both analytically and experimentally, in transient as well as steady state conditions, the straight bead problem in the case of realistic bead geometries. In Part I of this work, the theoretical formulation of the problem will be presented based on a consistent finite rotation, finite strain shell theory and a generalized Coulomb friction law. The significant increase in the model's complexity as compared to the model proposed by Wang [2] is justified by the arbitrariness of the bead's geometry and the consistency of the formulation. The experimental verification of the present model will be the object of the forthcoming Part II of this investigation.

The presentation starts with the variational formulation of the governing equations for the deformation of an initially flat sheet. A full Lagrangian description of the equations of motion is adopted with the reference state chosen to be the initially flat, stress free configuration of the sheet. After a brief derivation of an appropriate one dimensional (plane strain) large rotation and large strain shell theory valid for a wide class of rate independent incrementally linear solids, a penalty formulation for the contact part of the problem in the case of an arbitrary bead geometry is presented, together with a generalized Coulomb friction law, which is consistent with the full Lagrangian description of the governing equations adopted here.

The formulation is subsequently applied to the case of beads with rectangular cross section. The numerical solution technique is based on a Finite Element Method discretization of the governing nonlinear differential equations using an incremental Newton-Raphson approach. Both phases of the sheet deformation are analyzed: the "locking/clamping" phase as the binder forms the bead, and the "pulling" phase, which occurs as the main punch advances to form the part, causing bending and unbending of the sheet as it is pulled through the bead. The problem is solved incrementally, allowing the pulling phase to occur at any point during the locking process.

Of interest here are the strain distributions at the end of each phase as well as the restraining force provided by the drawbeads, i.e. the horizontal force-displacement relation during the "pulling" phase of the deformation. The first piece of information (strain distribution) is important in the determination of potential tearing failures for a particular bead design, while the second one (horizontal force-displacement relation) is necessary for the proper consideration of boundary conditions in modelling the actual sheet forming operations.

Of particular interest in the calculations will be the effects of variations in bead geometry, material properties, friction coefficient and boundary conditions (whether or not the motion of one end of the sheet is constrained by the presence of other beads). All the results presented here are based on the geometric and material properties of beads used in the experimental investigations to be reported in Part II of this work.

Contributed by the Materials Division for publication in the JOURNAL OF ENGINEERING MATERIALS AND TECHNOLOGY. Manuscript received by the Materials Division, December 26, 1985.

2 General Considerations

Interest in this work focusses on the deformation of an initially flat sheet under a straight lockbead. An appropriate plane strain, thick shell theory capable of incorporating large rotations and large strains and valid for a wide class of rate independent elastic-plastic materials will be employed. A general friction law consistent with the full Lagrangian description of the governing equilibrium equations adopted here, will also be presented. Although similar (but not as general) plane strain shell theories [3] and friction laws [4] have already been presented in the literature, the proposed model contains enough refinements to merit a separate presentation. An axisymmetric version of the present theory is given by Triantafyllidis and Samanta [5].

2.1 Equilibrium Equations and Strain Measures. Consider a planar curve C (identified with the reference line of the shell) where material points have position vector $\mathbf{r}(s)$ in the reference configuration, with s denoting arc length (see Fig. 1). Under the action of forces coplanar with C and moments with vectors perpendicular to its plane, the curve deforms to a new curve $\bar{C}(\bar{s})$ with $\bar{s}(s)$ the arc length on $\bar{C}$. The arc length parameters s in the undeformed configuration will play the role of material coordinate for the points of C. Variable's symbols surmounted by a bar ($\bar{}$) refer to the current configuration while omission of the bar denotes the corresponding quantity in the reference state.

Let $\mathbf{t}$ and $\mathbf{n}$ be the tangent and normal unit vectors to C. If $\mathbf{u}$ is the displacement of the material point s, one has

$$\bar{\mathbf{r}} = \mathbf{r} + \mathbf{u} = \mathbf{r} + v\mathbf{t} + w\mathbf{n} \tag{2.1}$$

where v and w are the components of $\mathbf{u}$ in the $(\mathbf{t}, \mathbf{n})$ basis. Using the Frenet formulas for the curve $C(\bar{C})$—see for example Goetz [6]—namely

$$d\mathbf{t}/ds = -\kappa\mathbf{n}\,(d\bar{\mathbf{t}}/d\bar{s} = -\bar{\kappa}\bar{\mathbf{n}}) \;,\; d\mathbf{n}/ds = \kappa\mathbf{t}\,(d\bar{\mathbf{n}}/d\bar{s} = \bar{\kappa}\bar{\mathbf{t}}) \tag{2.2}$$

where $\kappa(\bar{\kappa})$ is the curvature of $C(\bar{C})$, in conjunction with (2.1), the axial stretch ratio λ is found to be

$$\lambda \equiv d\bar{s}/ds = [(1+e)^2 + f^2]^{1/2}; \tag{2.3}$$

$$e \equiv dv/ds + \kappa w \;,\; f \equiv dw/ds - \kappa v$$

At this stage another kinematical quantity is introduced, the angle ϕ formed between $\mathbf{t}$ and $\bar{\mathbf{t}}$ (or equivalently between $\mathbf{n}$ and $\bar{\mathbf{n}}$) which from (2.1), (2.2) and (2.3) is found to satisfy

$$\cos\phi = (1+e)/\lambda \;,\; \sin\phi = -f/\lambda \tag{2.4}$$

Decomposing $\bar{\mathbf{t}}$ and $\bar{\mathbf{n}}$ with respect to the $\mathbf{t}$, $\mathbf{n}$ basis using (2.4) and employing also (2.2), the current curvature $\bar{\kappa}$ of $\bar{C}$ can be expressed as follows

$$\bar{\kappa} = \kappa/\lambda + [f\,de/ds - (1+e)df/ds]/\lambda^3 \tag{2.5}$$

Suppose that N, Q, and M are the current axial, shear and moment resultants at any point of $\bar{C}$, along $\bar{\mathbf{t}}$, $\bar{\mathbf{n}}$, $\bar{\mathbf{n}} \times \bar{\mathbf{t}}$, respectively, as shown in Fig. 1. The equilibrium equations for $\bar{C}$, subjected to distributed load $\mathbf{p}$ per unit current length with components $\bar{p}_t$ and $\bar{p}_n$ along the current tangential and normal directions, respectively, take the form

$$dN/ds + \bar{\kappa}\lambda Q + \lambda\bar{p}_t = 0 \;,\; dQ/ds - \bar{\kappa}\lambda N + \lambda\bar{p}_n = 0$$

$$dM/ds - \lambda Q = 0 \tag{2.6}$$

The following expression for the external virtual work is postulated

$$\text{E.V.W.} = M\delta\chi\Big|_{s_1}^{s_2} + Q(\delta\mathbf{u}\cdot\bar{\mathbf{n}})\Big|_{s_1}^{s_2}$$

$$+ N(\delta\mathbf{u}\cdot\bar{\mathbf{t}})\Big|_{s_1}^{s_2} + \int_{s_1}^{s_2} (\mathbf{p}\cdot\delta\mathbf{u})\lambda ds \tag{2.7}$$

where χ is the angle of rotation of a cross section initally along $\mathbf{n}$.

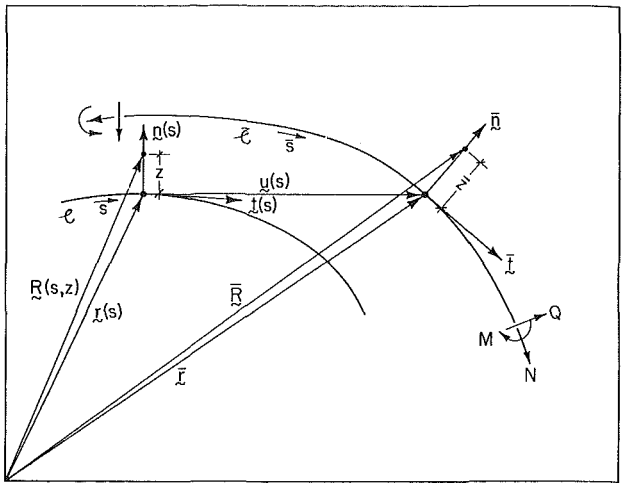

Fig. 1 Kinematic and dynamic variables related to the undeformed (C) and deformed ($\bar{C}$) configuration of the sheet

Denoting by ρ^*, γ^*, ϵ^* the linear in δv, δw, $\delta\chi$ quantities which are work conjugate to M, Q, N, respectively, the internal virtual work is assumed to be

$$\text{I.V.W.} = \int_{s_1}^{s_2} (M\rho^* + Q\gamma^* + N\epsilon^*)ds \tag{2.8}$$

From the principle of virtual work (I.V.W. = E.V.W.) and after making use of the equilibrium equations (2.6) as well as the kinematic ones (2.1)–(2.5) one obtains

$$\int_{s_1}^{s_2} \{M[\rho^* - d(\delta\chi)/ds] + Q[\gamma^* - \lambda(\delta\chi - \delta\phi)]$$

$$+ N[\epsilon^* - \delta\lambda]\}ds = 0 \tag{2.9}$$

At this point the additional assumption is introduced that the shear resultant Q is a workless (reaction) force and thus $\gamma^* = 0$. It then follows from (2.9), from the arbitrariness of the values of M, Q, N (and noting from (2.4) and (2.5) that $d\phi/ds = \lambda\bar{\kappa} - \kappa$) that ρ^* and ϵ^* are exact variations of the two strain measures ρ and ϵ given by

$$\rho^* = \delta\rho \;,\; \rho \equiv \bar{\kappa}\lambda - \kappa \;;\; \epsilon^* = \delta\epsilon \;,\; \epsilon \equiv \lambda - 1 \tag{2.10}$$

The attractive feature of this theory is that the work conjugate quantities to the current bending moment M and current axial force N are the exact variations $\delta\rho$ and $\delta\epsilon$ of the strain measures ρ and ϵ. What is more interesting is the fact that for a quite broad class of materials the rates $\dot{\rho}$ and $\dot{\epsilon}$ of these two strain measures appear in a natural way in the constitutive equations for M and N.

2.2 Constitutive Relations for the Stress Measures. Consider sheet metal of initial thickness h deforming under plane strain conditions and let C be the reference fiber curve of its undeformed cross section (see Fig. 1). If $\mathbf{R}$ is the position vector of material point A at a distance z from C in the reference configuration then

$$\mathbf{R}(s,z) = \mathbf{r}(s) + z\,\mathbf{n}(s) \;,\; -h/2 \le z \le h/2 \tag{2.11}$$

For the current configuration the cross-sectional normality assumption is adopted in agreement with the kinematical assumption $\gamma^* = 0$ (or $\chi = \phi$), made in the previous subsection. Cross sections normal to C in the undeformed state remain normal to $\bar{C}$ in the deformed one while they are allowed to expand or shrink. Consequently the current position vector $\bar{\mathbf{R}}$ can be expressed as

$$\bar{\mathbf{R}}(s,z) = \bar{\mathbf{r}}(s) + \bar{z}(s,z)\bar{\mathbf{n}}(s) \tag{2.12}$$

A Lagrangian formulation of the problem is adopted here with convected coordinates $\theta^1 = s$, $\theta^2 = z$. From (2.11) and (2.12) the nonzero covariant components of the undeformed

(deformed) metric tensor $G_{\alpha\beta} = \partial \mathbf{R}/\partial\theta^{\alpha} \cdot \partial \mathbf{R}/\partial\theta^{\beta}$ ($\bar{G}_{\alpha\beta} = \partial \bar{\mathbf{R}}/\partial\theta^{\alpha} \cdot \partial \bar{\mathbf{R}}/\partial\theta^{\beta}$)+ are found to be

$$G_{11} = (1+\kappa z)^2 \ , \quad (\bar{G}_{11} = [\lambda(1+\bar{\kappa}\bar{z})]^2)$$
$$G_{22} = 1 \ , \qquad (\bar{G}_{22} = (\partial\bar{z}/\partial z)^2) \tag{2.13}$$

where consistent with our assumption of zero transverse strain $\gamma^* = 0$ we have assumed $\partial\bar{z}/\partial s \cong 0$.

The rate of a field quantity is defined to be its derivative with respect to some monotonically increasing parameter characterizing the deformation history and is denoted by a dot superimposed on the symbol of the quantity in question. A fairly broad class of materials—which incorporates as special cases hyperelastic, hypoelastic as well as elastoplastic constitutive ones—is the class of incrementally linear materials. The corresponding constitutive equations relating the Kirchhoff stress rate $\dot{\tau}^{ij}$ to the rate of deformation tensor D_{ij} are of the form

$$\dot{\tau}^{ij} = L^{ijkl} D_{kl} \ , \quad (D_{ij} = \dot{\bar{G}}_{ij}/2) \tag{2.14}$$

where L^{ijkl} are the contravariant components of the incremental moduli tensor with respect to the current basis. The incremental moduli tensor may depend in general on the current metric, stress state, material properties and loading direction, and is usually taken to have the symmetries $L^{ijkl} = L^{klij} = L^{jikl} = L^{ijlk}$.

Assuming a state of plane stress (i.e., $\tau^{33} = 0$) at every point of the sheet, one deduces from (2.13) and (2.14)

$$\dot{\tau}^{11} = [\mathcal{L}/(\lambda(1+\bar{\kappa}\bar{z}))^4] D_{11};$$
$$\mathcal{L} \equiv L_{(1111)} - L_{(2211)} L_{(1122)}/L_{(2222)} \tag{2.15}$$

where $L_{(ijkl)}$ denote the physical components of $\mathbf{L}$.

Note that the current axial force and bending moment can be expressed as thickness integrals of the principal Cauchy stress $\sigma_{(11)}$

$$N = \int_{-h/2}^{h/2} \sigma_{(11)} \partial\bar{z}/\partial z \, dz \ , \quad M = \int_{-h/2}^{h/2} \sigma_{(11)} \bar{z} \partial\bar{z}/\partial z \, dz \tag{2.16}$$

Taking rates in (2.16), recalling that

$$\tau^{ij} = \sigma^{ij} [\det \bar{G}_{ij}/\det G_{ij}]^{1/2}$$

and making use of (2.13–2.15) one obtains

$$\dot{N} = C_{11}\dot{\epsilon} + C_{12}\dot{\rho} \ , \quad \dot{M} = C_{12}\dot{\epsilon} + C_{22}\dot{\rho} \ ,$$
$$C_{\alpha\beta} = \int_{-h/2}^{h/2} (\mathcal{L} + \tau_{(11)})(1+\kappa z)\bar{z}^{(\alpha+\beta-2)}/[\lambda(1+\bar{\kappa}\bar{z})]^2 dz \tag{2.17}$$

Observe that the strain rate measures appearing in (2.17) are exactly the rates of axial and bending strains found in the previous subsection. Moreover the symmetry of the incremental stiffness matrix $C_{\alpha\beta}$ in (2.17) is a consequence of the symmetry of the incremental moduli tensor $\mathbf{L}$ in (2.14).

For the special case of a hyperelastic material with strain energy density W per unit undeformed length s it can be shown that the constitutive equations assume the simplier form $N = \partial W/\partial\epsilon$, $M = \partial W/\partial\rho$. This result was first noted by Antman [3] who also found the strain measures introduced in (2.10) the most appropriate for a one dimensional elastic beam theory.

For the general rate independent material case the incremental relation between the stress and strain measures presented in (2.17) is the most useful form of the corresponding (shell) one dimensional constitutive equations, since it appears naturally in the incremental formulation of the governing equations (see (4.1)).

2.3 Appropriate Formulation for Contact and Friction. The determination of the surface part of the external virtual work term will take place in two parts. First the normal forces due to (frictionless) contact will be specified and subsequently the tangential (frictional) forces will be derived.

Constraining the sheet's middle surface to lie between the upper and lower drawbead surfaces is achieved via a penalty method formulation as follows: Assuming that the distances of a point M with material coordinate s on the sheet's middle surface from the bead's top and bottom surfaces are d_u and d_L, respectively, the contribution of the normal contact forces to the external virtual work is given by

$$(\text{E.V.W.})_{\text{contact}} = -k/2 \, \delta\left\{\int_{s_1}^{s_2} d_u^2 H(d_u) ds + \int_{s_1}^{s_2} d_L^2 H(d_L) ds\right\} \tag{2.18}$$

where d_u and d_L are functions of s, $\mathbf{u}$ as well as the geometry of the bead, and are signed negative if the material point M is outside the upper or lower bead surface, respectively. In addition $H(x)$ designates the Heaviside function (defined as $H(x) = 0$ for $x<0$ and $H(x) = 1$ for $x \geq 0$). The above assumption for the external virtual work term corresponds to a Winkler type foundation for the upper and lower bead surfaces, where the normal force per unit reference area is linearly proportional to the sheet's penetration depth, d_u or d_L, with coefficient of proportionality k. For adequately high values of the "foundation constant" k the upper and lower bead surfaces will behave almost rigidly.

The advantage of this type of formulation, usually called a penalty type of formulation in the literature (see for example Oden [4] and references quoted therein), apart from its realistic physical interpretation—in reality no contact can ever be perfectly rigid, there is always a small amount of elastic deformation involved—is that it simplifies considerably the resulting numerical calculations. Since the method decides automatically which part of the sheet is in contact with the rigid surfaces, it avoids more complicated iteration schemes usually employed in similar analyses of sheet metal forming processes (see for example Wang and Budiansky [7]).

In addition to the aforementioned advantages, the proposed formulation for the contact presents some additional benefits for the friction modeling. Denoting the distances d_u or d_L of a material point M from the top or bottom rigid surfaces by d for simplicity and observing that if the material point M is in contact with a rigid surface the normal force at the contact point is $\mathbf{t}_n = -k\, d\, H(d)\, \mathbf{n}$ (where $\mathbf{n}$ is the outward normal to the rigid surface in question) the corresponding contribution to the E.V.W. can be written as (see (2.18)).

$$(\text{E.V.W.})_{\text{contact}} = \int_{s_1}^{s_2} \{-k[d\, H(d)\delta d]_u - k[d\, H(d)\delta d]_L\} ds$$
$$= \int_{s_1}^{s_2} [(\mathbf{t}_n \cdot \delta\mathbf{u})_u + (\mathbf{t}_n \cdot \delta\mathbf{u})_L] ds \tag{2.19}$$

and hence since δd is linear in δv and δw by putting $\delta d = A\, \delta v + B\, \delta w$ one can find the outward normal and tangential unit vectors to the rigid surface to be given by

$$\mathbf{n} = A\,\mathbf{i} + B\,\mathbf{j} \ , \quad \mathbf{t} = \pm(-B\,\mathbf{i} + A\,\mathbf{j});$$
$$\delta d = \mathbf{n} \cdot \delta\mathbf{u} = A\, \delta v + B\, \delta w \tag{2.20}$$

The frictional force $\mathbf{t}_t$ at material point M is then specified as follows: Its magnitude t_t depends on the magnitude of the normal force t_n, as well as on the total distance u_T that the material point M has traveled on the rigid surface during contact. The proposed frictional constitutive law is a modified Coulomb law, of the type used by Oden and Pires [4]. Since at most one directional reversal is expected during the frictional process in the bead problems analyzed here, the constitutive equation for the friction assumes the form (see also Fig. 2)

+ Note: Here and subsequently greek indices range from 1 to 2, while latin indices range from 1 to 3.

$$f=\phi_\epsilon(u_T)\ ;\ 0\le u_T\le u_T^m \text{ and } \dot{u}_T(\tau)>0 \text{ for } t_0\le\tau\le t$$
$$t_t=-\mu t_n f\ ;\ f=[\phi_\epsilon(u_T^m)-(u_T^m-u_T)/\epsilon];\ u_T^m-\epsilon\phi_\epsilon(u_T^m)\le u_T\le u_T^m \qquad (2.21)$$
$$f=-[\phi_\epsilon(u_T^m-u_T-\epsilon\phi_\epsilon(u_T^m))];u_T\le u_T^m-\epsilon\phi_\epsilon(u_T^m)$$

where t_0 is the "time" at which frictional contact started at point M, u_T is the distance traveled on the surface of the punch by the material point in question from the time of initial contact, i.e.,

$$u_T=\int_{t_0}^{t}\dot{u}_T dt=\int_{t_0}^{t}(\mathbf{t}\cdot\dot{\mathbf{u}})dt^{+} \qquad (2.22)$$

and u_T^m is the distance at which a reversal in the direction of friction occurs, i.e., $\dot{u}_T(\tau)>0$ for $t_0\le\tau<\tau^m$, $\dot{u}_T(\tau)<0$ for $\tau^m<\tau$, and $\dot{u}_T(\tau^m)=0$, $u_T(\tau^m)=u_T^m$. In addition $\phi_\epsilon(x)$ is a monotonically increasing function of u_T with monotonically decreasing first derivative taken to satisfy $0\le\phi_\epsilon(x)\le 1$ with $\phi_\epsilon(0)=0$, $(d\phi_\epsilon/dx)(0)=1/\epsilon$, $d\phi_\epsilon/dx>0$, $d^2\phi_\epsilon/dx^2<0$, and also $\phi_\epsilon(x)\to 1$ as $x\to\infty$. Moreover ϵ is a small positive number and the family of curves ϕ_ϵ is assumed to have the property $\phi_\epsilon(x)\to 1$ as $\epsilon\to 0$.

In the above presented frictional law we have considered $\dot{u}_T(t_0)>0$. Such a condition is always possible in view of the sign arbitrariness in the definition of the tangent vector $\mathbf{t}$ to the rigid surface given in (2.20). Note also for the contact with friction case the distributed forces per unit reference area considered in Section 2 are $\lambda\bar{p}_n=t_n$, $\lambda\bar{p}_t=t_t$.

The frictional contribution to the external virtual work can then be put in the form

$$(\text{E.V.W.})_{\text{friction}}=\mu k\int_{s_1}^{s_2}\{[d_L H(d_L)f_L+d_u H(d_u)f_u](\mathbf{t}\cdot\delta\mathbf{u})\}ds \qquad (2.23)$$

where $f_L=f(u_T^L)\ \text{sgn}[\dot{\mathbf{u}}(t_0^L(s))\cdot\mathbf{t}(s)]$,

$f_u=f(u_T^u)\text{sgn}\ [\dot{\mathbf{u}}(t_0^u(s))\cdot\mathbf{t}(s)]$,

and where $u_T^L(t_0^L(s))$, $u_T^u(t_0^u(s))$ are the sliding distances on the lower and upper rigid surfaces from the onset of contact at times $t_0^L(s)$, $t_0^u(s)$, respectively, up to the current time t.

The weak formulation of the equilibrium equations is given by

$$\text{I.V.W.}=(\text{E.V.W.})_{\text{contact}}+(\text{E.V.W.})_{\text{friction}}=\text{E.V.W.} \qquad (2.24)$$

(see equations (2.8), (2.10), (2.18), and (2.23)). A discretized version of the rate form of (2.24) using finite elements constitutes the basis for the numerical solution of the bead problem analyzed here.

3 Formulation of the Boundary Value Problem—Localization Criterion

The bead's geometry is depicted in Fig. 3. Note that for the idealized bead geometry (shell idealized by its centerline) the actual dimensions are augmented by half a sheet thickness. The lower (male) bead has a cross-section of width $2(B_1+R_1)$ and a depth of H_1+R_1, while the upper (female) bead has a cross section of width $2B_2$ and a depth of H_2+R_2 where R_1 and R_2 are the radii of curvature at the corners of the lower and upper beads, respectively, and h is the initial sheet thickness. In its stress-free configuration the sheet's centerline touches the upper and lower bead as shown in Fig. 3, while the sheet's total length is $2L$. In the applications studied here we take $40h\le 2L\le 60h$, which is a reasonable value for the interbead distance in most automotive die configurations.

The deformation processess takes place in two stages. During the first stage the male bead advances to its final position (punch advance $H=H_1+R_1$), simulating the binder locking the sheet into place. During the second stage of deformation, which occurs during the main forming operation, the right end is drawn inwards by an amount Δ. Boundary conditions at the edges of the sheet are therefore determined as follows: During the first stage of deformation the sheet does not slide across the binder surface, hence the right edge is held fixed ($v=w=w'=0$ at $s=L$). During the second stage the right edge is displaced inward as material is drawn through the bead ($v=\Delta$, $w=w'=0$ at $s=L$). Two boundary condition cases are considered for the left edge of the sheet; the "clamped" case ($v=w=w'=0$ at $s=-L$) simulating the presence of other beads to the left of the present one, and the "free" case ($w=w'=0$ at $s=-L$).

A finite strain version of the J_2 flow theory of plasticity is employed in the present calculations. Since the theory has already been presented elsewhere in the literature [8] only a brief description is given in appendix $A1$ concerning the determination of the 3-dimensional incremental moduli $\mathbf{L}$ appearing in Section 2.3.

Finally a remark of interest about the numerical calculation of the localization of deformation that occurs during the deformation of the sheet. Failure by localization of deforma-

+ Note: $\dot{\mathbf{u}}$ represents the relative velocity between the point M and the punch surface.

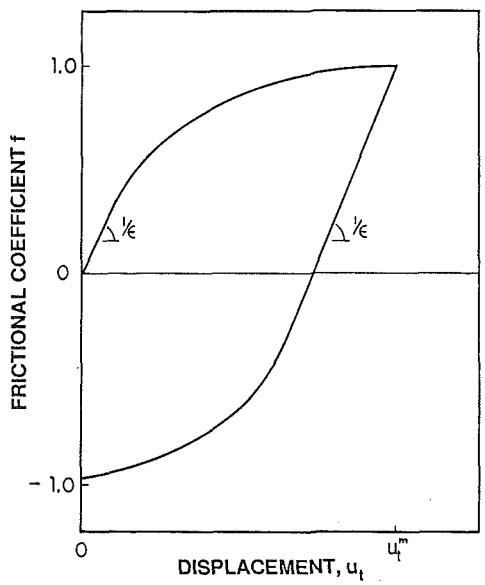

Fig. 2 Frictional coefficient f versus displacement with one sliding direction reversal at $u_T=u_T^m$

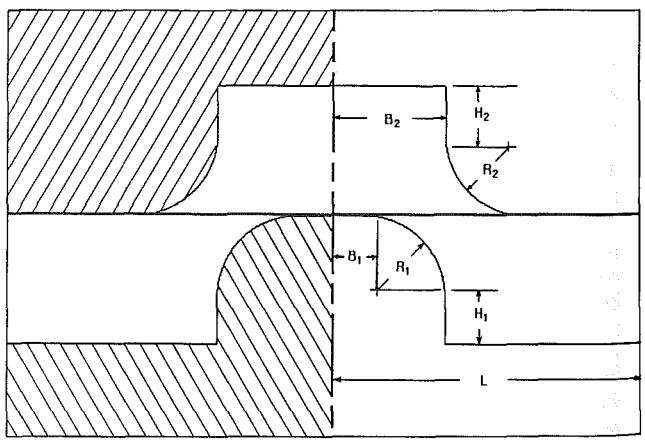

Fig. 3 Geometric variables of the flat bead

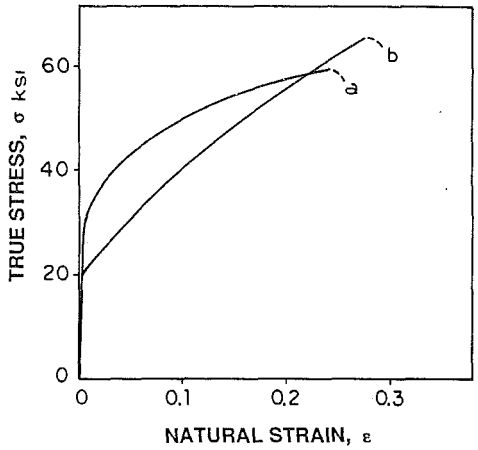

Fig. 4 True stress versus natural strain curves for (*a*) mild steel and (*b*) brass

tion is the only type of failure that is considered in this process and its knowledge is of paramount importance for the successful design of such a bead. From a mathematical standpoint this type of failure occurs when the corresponding incremental equations of equilibrium admit a singular point. Using the rate form of (2.6) in conjunction with (2.17) and writing all the corresponding equations in an updated Lagrangian formulation, the corresponding governing equations admit a singular point when

$$\bar{C}_{11}\bar{C}_{22}-(\bar{C}_{12})^2=0\ ;\ \bar{C}_{\alpha\beta}=\int_{-h/2}^{h/2}\frac{(\mathfrak{L}+\sigma_{(11)})\bar{z}^{\alpha+\beta-2}}{(1+\bar{\kappa}\bar{z})^2}d\bar{z} \tag{3.1}$$

for as long as the left-hand side of the above equation is positive, no localization instability occurs. The first time (as the "time" parameter for this deformation process increases monotonically) that the above criterion is met for a given point $s=s^*$, i.e., the first time that the incremental equilibrium equations for the shell admit a singular point, localization failure is considered to have occurred.

4 Numerical Method

The finite element method (F.E.M.) is employed in order to solve the boundary value problem discussed in the previous section, i.e. the deformation of an initially flat sheet of thickness h due to the advance by a distance H of the male bead and the subsequent pulling by a distance Δ of one of its ends. The basis for the solution algorithm is the incremental virtual work formulation derived from (2.24) namely

$$[(\text{I.V.W.})'-(\text{E.V.W.})']\Delta t=-(\text{I.V.W.}-\text{E.V.W.}) \tag{4.1}$$

where $(')$ denotes differentiation with respect to the monotonically increasing time-like parameter t which is identified with H (the upper bead displacement) during the first step of the deformation and with Δ (the horizontal displacement of the right edge) during the second stage of the deformation. It can be seen from the strain-displacement equations (2.3), (2.5), and (2.10) that up to the second order spatial derivatives of the horizontal and vertical displacements v and w are involved. Thus C^1 shape functions i.e., functions with continuous derivatives are employed here. Within each element $v(s)$ and $w(s)$ are approximated by Hermitian cubics and a four point Gauss-Legendre numerical integration scheme is used.

A power law type mesh modification near the ends of the sheet is adopted namely

$$r_N=A(r_0)^\beta+B \tag{4.2}$$

where r_N is the new (refined) coordinate and r_0 the one corresponding to a uniform subdivision in $N+1$ points of the interval $[-L,L]$. The mesh refinement exponent is denoted by β, and in all the calculations reported here $1\le\beta\le 3$.

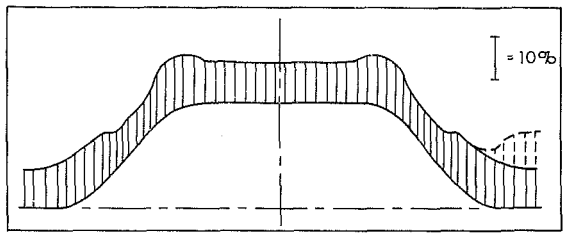

Fig. 5(*a*) Strain distributions over the sheet for bead *A*, mild steel, clamped boundary condition, after punching (solid line) and pulling (dashed line)

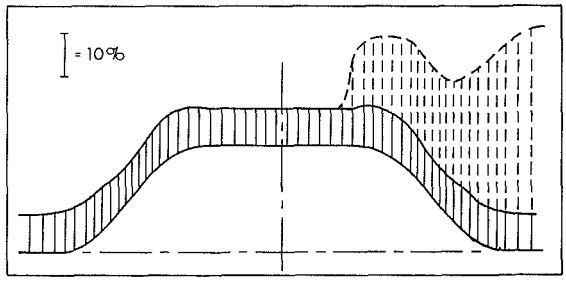

Fig. 5(*b*) Strain distributions over the sheet for bead *A*, brass, clamped boundary condition, after punching (solid line) and pulling (dashed line)

An incremental Newton-Raphson algorithm based on (4.1) is adopted for the solution of the problem. The step size Δt required for the convergence of the algorithm depends on the presence of friction (i.e., $\mu=0$ or $\mu>0$). For the case $\mu=0$, Δt may be taken as large as $0(h)$. For the case $\mu>0$ it is found that $\Delta t=0(10^{-3}h)$ is necessary. In all subsequent calculations the sheet was taken to be transversely isotropic, i.e., $R=1$.

The function $\phi_\epsilon(x)$ involved in the modified Coulomb friction law outlined in (2.21) is taken to be

$$\phi_\epsilon(x)\equiv 2/\pi\ \tan^{-1}(x/\epsilon) \tag{4.3}$$

with the value of ϵ taken to be $\epsilon = 0.001$ in the numerical calculations presented here. The friction coefficient μ is taken to be $\mu=0.1$ or 0.2.

The "foundation constant" k (see (2.18) for its definition) is taken to be $k/Eh=50$. For this value of k the penetration distance d_u or d_L never exceeds 10^{-2} h. All the numerical calculations presented here are performed using $50 \le N \le 80$ elements.

Finally, the onset of localization is detected by checking the sign of the determinant in (3.1) at every integration station in every element of the shell. The first time during the deformation process that a non-positive value for the aforementioned determinant is found signals the onset of a localization in the deformation process and the calculation is terminated. It should also be mentioned at this point that all the integrals through the thickness included in the computations (see equation (2.16), (2.17)) are numerically evaluated using a 21 point Simpson rule.

5 Results and Discussion

As explained in the introduction, of interest here are the strain distributions over the sheet at the end of the "locking" and "pulling" phases of deformation, as well as the normal and horizontal force-displacement relations. The present calculations investigate the effects of bead geometry, material properties, friction coefficient, and boundary conditions on the aforementioned strain distributions and force-displacement relations.

Two different rectangular bead geometries, which were employed in the experimental investigations to be reported in Part II of this work, are analyzed here. The first, to be subsequently termed bead A for simplicity, is an almost square bead

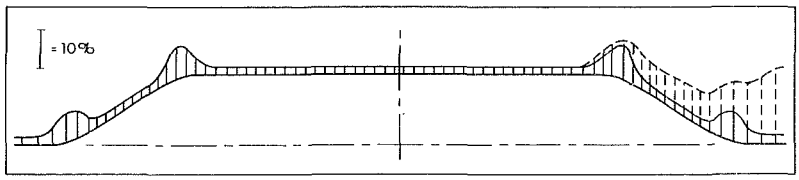

Fig. 6 Strain distributions over the sheet for bead *B*, mild steel, clamped boundary condition, after punching (solid line) and pulling (dashed line)

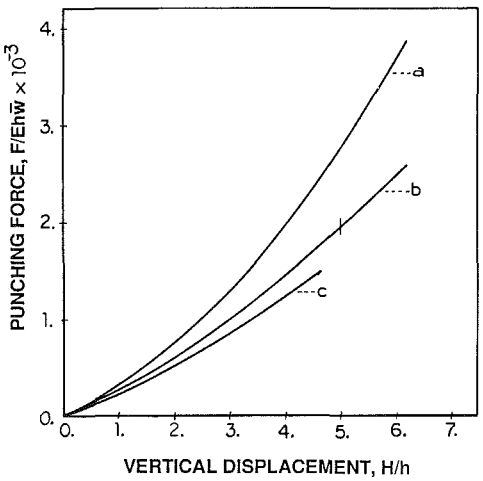

Fig. 7 Nondimensionalized punching force $F/Eh\bar{w}$ ($\bar{w}$ = bead width) versus vertical displacement H/h for clamped boundary condition: (*a*) bead *A*, brass; (*b*) bead *A*, mild steel; (*c*) bead *B*, mild steel

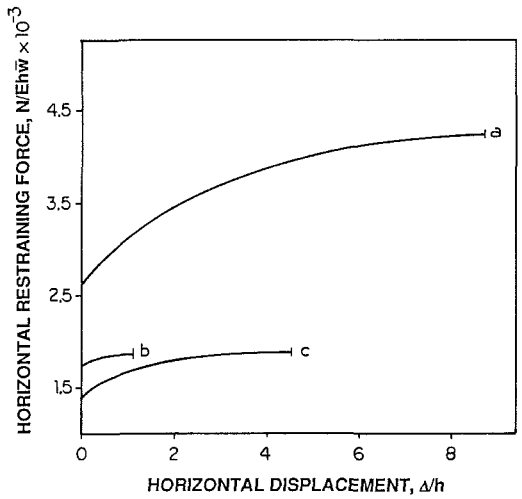

Fig. 8 Nondimensionalized horizontal restraining force $N/Eh\bar{w}$ versus horizontal displacement Δ/h for clamped boundary condition: (*a*) bead *A*, brass; (*b*) bead *A*, mild steel; (*c*) bead *B*, mild steel

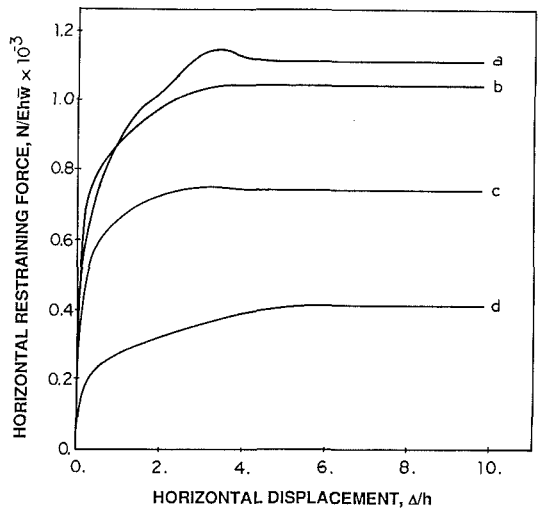

Fig. 9 Nondimensionalized horizontal restraining force $N/Eh\bar{w}$ versus horizontal displacement Δ/h for free boundary condition: (*a*) bead *A*, brass, $\mu = 0.1$; (*b*) bead *A*, mild steel, $\mu = 0.2$; (*c*) bead *A*, mild steel, $\mu = 0.1$; (*d*) bead *B*, mild steel, $\mu = 0.1$

of dimensions $R_1 = R_2 = 4.66h$, $B_1 = 4.16h$, $B_2 = 8.83h$, $H_1 = 1.56h$, $H_2 = 5.66h$. The second one, hereafter called bead B, is a flatter bead of dimensions $R_1 = R_2 = 4.66h$, $B_1 = 13.0h$, $B_2 = 18.32h$, $H_1 = 0$, $H_2 = 5.66h$. In both cases the nondimensionalization was based on a sheet thickness $h = 0.030''$.

The materials employed here are mild steel and brass, whose uniaxial true stress—natural strain curves are shown in Fig. 4. As explained in Section 3, two different boundary conditions at the left edge of the sheet ($s = -L$) are investigated, one corresponding to a clamped edge and one to a traction free edge. Finally, the friction coefficients employed in the calculations are $\mu = 0.1$ and $\mu = 0.2$.

The mid-surface strain distributions over the sheet for the case of bead A with a clamped left edge are shown at the end of the "locking" (solid line) and "pulling" (dashed line) phases of deformation in Fig. 5(*a*) for mild steel and Fig. 5(*b*) for brass. In each case, a friction coefficient of $\mu = 0.1$ was used. The "pulling" phase of deformation was continued until a localization of deformation occurred at some point in the shell (see discussion of Section 3). As expected due to the higher hardening in the brass sheet, its right end was pulled a distance $\Delta_{cr} = 8.8h$ before localization occurred, as opposed to the mild steel sheet which failed at $\Delta_{cr} = 1.1h$. Figures 5(*a*) and 5(*b*) also demonstrate the effect of "pulling" on the strain distribution over the sheet. In both cases, the redistribution of strains never affects the left half of the sheet, whose points practically do not move. Even in the case of brass where a significant displacement of the right end is possible before failure, points in the left two thirds of the sheet remain unaffected, a fact due both to the clamping restriction at the left end and to the presence of friction.

Keeping the boundary conditions and friction coefficient the same, the above calculations were repeated for the case of mild steel using bead *B*. The corresponding strain distributions are depicted in Fig. 6. Due to the lower mid-surface strains at the end of the locking phase of deformation, a higher critical displacement $\Delta_{cr} = 4.5h$ was required to initiate localization. In every case, the point at which localization began was the right edge of the rightmost radius in the bead.

For the above three cases the (nondimensionalized) punching force $F/Eh\bar{w}$* versus (nondimensionalized) vertical displacement H/h relation is depicted in Fig. 7. As expected, flattening the bead's profile leads to a lower punching force $F/Eh\bar{w}$ due to the correspondingly smaller strains, while changing materials from steel to brass raises $F/Eh\bar{w}$. All the calculations reported in Fig. 7 were performed using a friction

*Note: $\bar{w}$ is the constant (due to plane strain conditions) sheet width.

coefficient $\mu = 0$ to improve computational speed, as friction was seen to play a negligible role during "punching" with both ends of the sheet clamped. Indeed repeating the computations for bead A with mild steel, clamped edges and $\mu = 0.1$ showed no appreciable difference in the results during the "punching" phase of deformation. Of course during the "pulling" phase friction plays a very important role as Figs. 5(*a*), 5(*b*), and 6 show a significant strain increase in the areas of high relative motion between the bead and sheet.

The (nondimensionalized) horizontal force $N/Eh\bar{w}$ versus (nondimensionalized) horizontal displacement Δ/h relations for the three aforementioned cases are shown in Fig. 8. This information is of great importance in modelling the actual stamping processes in sheet forming, since it gives the exact boundary condition resulting from a given bead design.

The calculations were repeated for the case where the left edge of the sheet ($s = -L$) slides freely. The horizontal force $N/Eh\bar{w}$ versus horizontal displacement Δ/h diagram is presented in Fig. 9 for the four cases: bead A, mild steel, $\mu = 0.1$ and $\mu = 0.2$; bead A, brass, $\mu = 0.1$; and bead B, mild steel, $\mu = 0.1$. Note in all cases a steady state condition of deformation is reached after the horizontal displacement Δ becomes large ($\Delta \cong 4h$).

6 Concluding Remarks

The formulation of the bead problem assumes the sheet to behave as a shell (as opposed to membrane), allowing for bending as well as stretching stiffness. The additional complexity of this model compared to previous membrane models seems necessary when considering the sharp corners found in typical automotive beads. Bending effects become increasingly important when friction is reduced, and when the sheet is pulled over large distances through the bead.

Numerical results given here demonstrate several trends. Deep, narrow beads are seen to provide the greatest restraining force during the pulling phase of deformation, but also have the greatest risk of sheet failure during the locking phase, especially when the binder surface includes more than one bead. Wide, shallow beads produce little risk of tearing during locking, since strains across the sheet are lower and more uniform, and also allow material to pull through more easily as the panel is formed. Higher work hardening rate materials such as brass allow far higher strains before tearing, hence deeper beads may be used. As compared to geometric and material changes, the friction coefficient has little effect on the restraining force and on the sheet failure at the pulling stage. A lower coefficient was seen to produce more even strain distribution across the sheet, allowing material to slip over sharp corners where it would otherwise have torn.

The present investigation, in conjunction with the forthcoming experimental verification in Part II of this work, serves a dual purpose. Firstly, it provides a realistic and accurate model for the study of a complex and important technological problem, and secondly it provides the die designer with a reliable analytical tool for the design of straight beads, a task performed to date on an expedient trial and error basis.

Acknowledgments

The authors wish to acknowlege the support of Messrs. J. Heetderks and D. Raffin of Ford Body and Assembly Operations and the financial support from Advanced Engineering and Research funding, Ford Motor Co.

References

1 Nine, H. D., "Drawbead Forces in Sheet Metal Forming," *Mechanics of Sheet Metal Forming*, Plenum Press, New York, 1978, pp. 203–211.

2 Wang, N. M., "A Mathematical Model of Drawbead Forces in Sheet Metal Forming," GMR-3644, April 29, 1981.

3 Antman, S. S., "General Solutions of Plane Extensible Elasticae Having Nonlinear Stress-Strain Laws," *Quarterly of Applied Mathematics*, Vol. 26, 1968, pp. 35–47.

4 Oden, J. T., and Pires, E. B., "Nonlocal and Nonlinear Friction Laws and Variational Principles for Contact Problems in Elasticity," ASME *Journal of Applied Mechanics*, Vol. 50, No. 1, Mar. 1983, pp. 67–76.

5 Triantafyllidis, N., and Samanta, S. K., "Bending Effects on Flow Localization in Metal Sheets," *Proceedings of the Royal Society*, London, A, 406, pp. 205–226, 1986.

6 Goetz, A., *Introduction to Differential Geometry*, Addison-Wesley Pub. Co., London, 1970.

7 Wang, N. M., and Budiansky, B., "Analysis of Sheet Metal Stamping by a Finite Element Method," ASME *Journal of Applied Mechanics*, Vol. 45, No. 1, Mar. 1978, pp. 73–82.

8 Hutchinson, J., "Numerical Solutions of Nonlinear Structural Problems," AMD, Vol. 17, ASME, N.Y., 1973.

APPENDIX

Three-dimensional incremental moduli for J_2 flow theory are

$$L^{ijkl} = L_e^{ijkl} - \frac{\alpha (L_e^{ijmn} \partial\phi/\partial\sigma^{mn})(L_e^{pqkl} \partial\phi/\partial\sigma^{pq})}{\sigma^2/(1/E_t - 1/E) + \partial\phi/\partial\sigma^{mn} L_e^{mnpq} \partial\phi/\partial\sigma^{pq}} \tag{A.1}$$

where $\alpha = 1$ for plastic loading and $\alpha = 0$ otherwise. In the above equations, L_e denote the isotropic elastic moduli, i.e.

$$L_e^{ijkl} = (E/(1+\nu))[(g^{ik}g^{jl} + g^{il}g^{jk})/2 + (\nu/(1-2\nu))g^{ij}g^{kl}] \tag{A.2}$$

with E, ν the Youngs modulus and Poisson's ratio, respectivley.

The equivalent stress σ for the transversely isotropic material with anisotropy ratio R is given by

$$\sigma^2 = 2\phi = \frac{(\sigma^{<11>} - \sigma^{<33>})^2 + (\sigma^{<22>} - \sigma^{<33>})^2 + R(\sigma^{<11>} - \sigma^{<22>})^2 + 2(1+2R)(\sigma^{<12>})}{1+R} \tag{A.3}$$

For a material with a uniaxial true stress σ natural strain ϵ curve $\sigma = \sigma(\epsilon)$ and a yield stress σ_y, the tangent and secant moduli are given by

$$E_s = \sigma/\epsilon\ , \qquad E_t = d\sigma/d\epsilon \qquad \text{for } \sigma > \sigma_y$$
$$E_s = E_t = E \qquad \text{for } \sigma < \sigma_y \tag{A.4}$$